Mapping Cloudburst-Induced Ground Deformation in the Himalaya: Sentinel-1 InSAR Analysis of the July 2025 Manali Event

Shivanshu Tiwari
Department of Applied Mathematics
Defence Institute of Advanced Technology (DIAT), DRDO
Pune, Maharashtra, India shivanshu.mam24@diat.ac.in

Bharath Ramkrishna
Department of Applied Mathematics
Defence Institute of Advanced Technology (DIAT), DRDO
Pune, Maharashtra, India rambharath@diat.ac.in

doi: https://doi.org/10.37285/bsp.SACAD2025.72

***Abstract*—Extreme precipitation events in the Himalaya are becoming more frequent and destructive, driven by a combination of monsoon intensification, changing atmospheric moisture dynamics, and fragile mountain geomorphology. Cloudbursts in particular deliver intense rainfall over short durations, often overwhelming steep slopes and river systems, and triggering flash floods, debris surges, and subtle to catastrophic land-surface deformation. Traditional field-based observations struggle to capture these rapid and spatially distributed terrain responses due to limited accessibility, safety constraints, and coarse monitoring networks. This creates a critical knowledge gap in understanding the immediate geomorphic impact of extreme rainfall events in remote mountain belts.**

In this study, we analyzed the 1st July 2025 Manali cloudburst using a focused Differential InSAR (D-InSAR) approach applied to Sentinel-1 SAR acquisitions spanning May 2024 to July 2025. A carefully chosen pre-event reference period (January 2025) and paired ascending/descending interferograms were processed in ESA SNAP to rapidly isolate short-term deformation rather than rely on long-window PS-InSAR or SBAS methods. This deliberately event-centric strategy enhances sensitivity to cloudburst triggered displacement rather than long-term tectonic or seasonal signatures.

The resulting displacement maps reveal spatially coherent subsidence zones along river terraces, alluvial fans, and saturated slopes, with localized uplift patches observed along ridge slopes likely associated with transient elastic ground response and hydro-mechanical loading. These patterns collectively illustrate how intense rainfall pulses propagate mechanical stress through Himalayan hill slopes, accelerating slope adjustments and heightening exposure for settlements, infrastructure, and tourism corridors.

***Index Terms*—Remote sensing, Synthetic aperture radar (SAR), interferometric SAR (InSAR), Ground deformation mapping, Extreme rainfall events, Cloudburst hazards.**

I. INTRODUCTION

The Himalayan region, forming one of the youngest and most tectonically active mountain ranges on Earth, is highly vulnerable to hydro-meteorological hazards. The combination of steep topography, fragile geological formations, and intense monsoonal rainfall frequently triggers landslides, debris flows, and flash floods. Among these hazards, cloudbursts represent one of the most destructive phenomena. Cloudbursts are short-duration, high-intensity rainfall events, often exceeding 100 mm within an hour, that can release massive amounts of water over a confined area. Their occurrence in the Himalayas has been increasingly reported in recent decades, raising concerns regarding both climate variability and anthropogenic pressure on fragile mountain ecosystems [1, 2]. Monitoring such events remains a scientific challenge due to their localized nature and the complex terrain of the Himalayas. Conventional hydrological and meteorological networks often lack the spatial density to capture these highly localized events. Similarly, field-based surveys, though precise, are constrained by accessibility, time, and safety, and cannot capture the full spatial extent of terrain deformation. This knowledge gap necessitates the adoption of advanced, wide-coverage observation tools. Satellite-based Synthetic Aperture Radar (SAR) has emerged as a transformative remote sensing technology because it provides all-weather, day-and-night coverage, making it especially effective during the monsoon season when optical observations are obstructed by persistent cloud cover [3]. More importantly, Interferometric SAR (InSAR) enables the detection of ground displacement with centimeter-to-millimeter precision, which is crucial in steep mountain regions where even minor deformations may serve as precursors to slope failures. InSAR has therefore become a reliable tool for hazard monitoring, particularly in mountainous environments. On 1st July 2025, a severe cloudburst occurred in Manali, situated in the Kullu Valley of Himachal Pradesh. This event triggered intense flash floods, caused widespread infrastructure damage, and raised critical concerns regarding slope stability in a region characterized by dense human settlements, thriving tourism, and vulnerable infrastructure [4]. While preliminary ground observations indicated localized slope failures and surface cracks, they lacked the synoptic perspective required to assess valley-wide impacts. The objective of this study is to detect and quantify ground deformation associated with the July 2025 Manali cloudburst using Sentinel-1 SAR imagery. By analyzing both ascending and descending acquisitions from May 2024 to July 2025, the study aims to generate displacement maps that highlight zones of subsidence, uplift, and slope instability directly linked to the event. The novelty of this work lies in integrating SAR based deformation mapping with the hazard-specific context of an extreme rainfall event in the Himalayas. Beyond its scientific contribution, this study underscores the potential of satellite-based hazard monitoring in fragile mountain environments. The results are expected to inform slope stabilization strategies, urban planning, and infrastructure protection. In the long term, incorporating such methods into regional disaster management frameworks could enhance early warning systems and reduce the socio-economic vulnerability of Himalayan communities. The utility of Synthetic Aperture Radar (SAR) and its interferometric variants (InSAR) for quantifying ground deformation has been extensively demonstrated during the last two decades. Fundamental reviews and methodological studies describe the physical basis of phase measurement, the principal error sources (temporal decorrelation, geometric decorrelation, and atmospheric delays), and common processing stages (coregistration, interferogram formation, filtering, phase unwrapping, and time-series inversion). These foundational works provide practical guidance for monitoring deformation with centimeter-to-millimeter precision when appropriate processing and corrections are applied [6]. Two time-series InSAR paradigms have become the standard for hazard applications: the Small-Baseline Subset (SBAS) method and Permanent Scatterer (PS) approaches. SBAS reduces decorrelation and atmospheric noise by forming many small-baseline interferograms and then solving a temporal inversion for displacement, which is particularly effective for distributed scatterer fields and large-scale mapping. PS approaches, by contrast, focus on temporally stable radar scatterers and produce highly precise pointwise displacement histories that are robust against temporal decorrelation and atmospheric artifacts; both approaches have been refined and adapted for vegetated, mountainous environments [7]. Phase filtering and noise reduction techniques are essential preconditions to reliable unwrapping and subsequent displacement retrieval. Adaptive filters such as the Goldstein filter reduce phase noise and improve unwrapping success, which in turn strengthens the reliability of subsequent time-series inversion. Practical processing pipelines therefore combine noise-aware filtering, coherence masks, and tropospheric correction approaches to limit the contamination of true deformation signals by non-tectonic noise [8]. Software toolkits and processing pipelines have also matured. StaMPS (Stanford Method for Persistent Scatterers) and other PS/SBAS implementations provide accessible, tested workflows for PS selection, atmospheric estimation, and time-series inversion. Manuals and community resources for these tools describe best practices for mountainous terrain, including guidance on coherence thresholds, phase variance criteria, and strategies for multi-orbit (ascending + descending) analysis. Using these established toolchains (SNAP/ISCE + StaMPS/StaMPS-manual) allows reproducible, semiautomated analyses suitable for case studies and regional mapping [9].

Regionally focused studies in the Indian Himalaya and adjacent mountain belts demonstrate the practical value and limitations of Sentinel-1 time-series InSAR.

Multi-temporal Sentinel-1 analyses in Mussoorie (Uttarakhand) and other Himalayan localities have detected seasonal acceleration during monsoon months, identified active slope sectors, and quantified displacement rates that are consistent with rainfall forcing and hydrological changes. These case studies show that the Sentinel-1 revisit cadence and C-band sensitivity enable timeseries capture of both slow and seasonal motion, though steep slopes and dense vegetation can reduce coherent pixel density and demand tailored processing strategies (e.g., PS selection, spatial smoothing, and incorporation of external data) [10]. Several recent Himalayan works explicitly combine multiorbital InSAR with field investigations and rainfall analysis. For example, multi-orbit PS studies in Sikkim demonstrate that ascending and descending data together improve the interpretation of deformation vectors (helping to disambiguate vertical vs. horizontal components) and that even limited ground checks significantly enhance the credibility of remote detections. These multi-data, multi-orbit approaches are particularly relevant for urban-adjacent slopes, where small displacement magnitudes can rapidly translate into serious infrastructure risk [6]. Several large-scale applications demonstrate the scalability of SBAS and PS-InSAR for transport and infrastructure corridors. For example, Solari et al. (2019) processed long Sentinel-1 time-series to monitor slope instabilities affecting roads and railways, showing how interferometric analysis can support hazard management in transportation planning. Similarly, Bekaert et al. (2015) applied SBAS-InSAR to hundreds of SAR images over Northern California, successfully detecting and characterizing multiple active landslides across complex mountainous terrain. These works illustrate that dense Sentinel-1 archives, when processed with robust SBAS pipelines, can systematically identify deformation clusters at regional scales and are directly relevant to cloudburst-prone areas of the Himalaya [11, explicitly focus on immediate deformation after cloudbursts — combining ascending + descending Sentinel-1 stacks and supporting rainfall/field data — are comparatively rare. The present study of the 1st July 2025 Manali cloudburst is positioned to fill this targeted gap by applying a deliberate pre/post multi-orbit InSAR strategy and integrating satellite and ground observations to map and interpret the 12]. Despite the demonstrated capabilities, a careful reading of the literature surfaces two important gaps relevant to cloudburst. First, most Himalayan InSAR work focuses on seasonal or long-term slope motion rather than the immediate, short-duration geomorphic response to an extreme rainfall event (cloudburst). Secondly, many analyses either rely on a single orbit or on multi-year stacks, and do not explicitly design pre-event vs immediate post event comparisons that isolate deformation attributable to a single extreme rainfall pulse. As a consequence, the spatial footprint and short-term temporal evolution (days to months) of cloudburst-induced deformation remain relatively under explored. Addressing these gaps requires deliberate selection of pre/post windows, multi-orbit analysis, and integration of auxiliary hydrometeorological data [6, 10]. Methodologically, case studies of cloudburst-induced deformation benefit from a hybrid strategy: (1) construct dense interferogram stacks for pre-event and post-event windows; (2) assess coherence and select PS vs SBAS processing depending on scatterer density;
(3) apply robust phase filtering and tropospheric corrections where possible; (4) perform ascending and descending processing to retrieve LOS displacements from different viewing geometries and infer vertical/horizontal components; and (5) integrate optical imagery, DEM differencing, and rainfall maps to contextualize the deformation patterns. This combined approach has been shown to increase confidence in attributing deformation to hydrometeorological forcing and to improve the practical utility of results for hazard mitigation in summary, the existing literature provides strong methodological foundations (PS/SBAS, filtering, tropospheric mitigation, multiorbital analysis) and successful regional examples (Mussoorie, Gangtok, Darjeeling–Sikkim) that can be adapted for cloudburst case studies. However, targeted pre/post-event InSAR analysis that
event-specific deformation footprint.

II. Study Area and Event Description

The study focuses on Manali, a well-known hill town in the upper Beas River valley of Himachal Pradesh, India. Geographically, the region lies between 32.20°N–32.35°N latitude and 77.05°E–77.25°E longitude, covering the densely populated Manali township and the adjoining river catchments. The elevation ranges from 2,000 m in the valley floor to above 5,000 m along surrounding ridges, producing steep relief and narrow valleys [13]. This rugged geomorphology makes the area highly sensitive to extreme hydrometeorological events. Slopes are often mantled by loose colluvium and glacial deposits, while the Beas River and its tributaries cut deeply incised channels. Settlements, road networks, and tourism infrastructure are concentrated along the valley bottom, making them directly vulnerable to slope failures and flash floods. The July 2025 cloudburst generated intense rainfall within a confined catchment, leading to sudden flooding, debris flow activity, and damage to both natural slopes and built-up areas. Such events highlight the fragile coupling between climate extremes and terrain instability in the Himalayan context. The defined Area of Interest (AOI) therefore, provides an ideal setting to evaluate ground deformation using Sentinel-1 SAR, as the radar signals are less hindered by cloud cover and can capture subtle surface displacement even in challenging mountain environments.

- Orbit Ephemerides (POE) provided by the European Space Agency (ESA)
- **Reference Data:** 30 m Shuttle Radar Topography Mission (SRTM) Digital Elevation Model (DEM) used for topographic correction

For topographic phase removal and terrain correction, the 30 m SRTM DEM was utilized to minimize elevation-induced phase errors. The dual-orbit (ascending and descending) configuration allowed cross-validation of deformation patterns and enhanced sensitivity to vertical and horizontal motion components.

The overall data composition is summarized in Table I, which highlights the coverage period, acquisition mode, and orbit geometry employed in this study.

IV. METHODOLOGY

The interferometric Synthetic Aperture Radar (InSAR) workflow consists of a sequence of processing steps designed to extract ground deformation from complex radar acquisitions. The overall workflow is shown in Fig. 1. The key mathematical formulations used in this study are summarized below.

III. DATA AND DATASET SPECIFICATIONS

A dataset of Sentinel-1A/B Synthetic Aperture Radar (SAR) Single Look Complex (SLC) images was acquired, covering the period from May 2024 to July 2025. Both ascending and descending passes were included to capture displacement from different line-of-sight (LOS) geometries and improve deformation interpretation.

The specifications of the Sentinel-1 dataset used in this study are summarized below:

- **Acquisition Mode:** Interferometric Wide (IW)
- **Polarization:** VV

TABLE I
SPECIFICATIONS OF SENTINEL-1 SAR DATASET USED IN THE STUDY

S.No	No. of Images	Duration	Specification	Pol.	Flight Dir.
01	12	May 2024-july 2025	S1A_IW_SLC	VV+HH	Ascending
02	12	May 2024-july 2025	S1A_IW_SLC	VV+HH	Descending

- **Spatial Resolution:** Approximately 20 m in range and 5 m in azimuth
- **Revisit Cycle:** 6–12 days
- **Orbits:** Precise

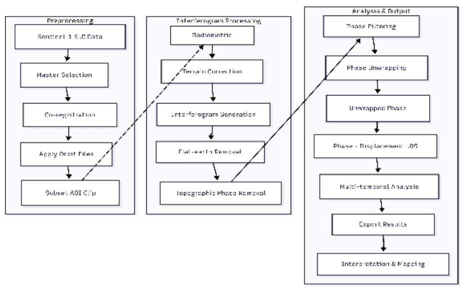

Fig. 1. Workflow of the InSAR processing chain for detection of ground deformation.

A. *Overall Interferometric Phase Model*

The measured interferometric phase in a pixel can be represented as the sum of several components: deformation, topography, flat-earth geometry, orbital errors, atmospheric delays, and noise. Understanding these contributions is essential because the deformation signal is often much smaller than atmospheric or orbital effects [1].

$\phi_{meas} = \phi_{def} + \phi_{topo} + \phi_{flat} + \phi_{orb} + \phi_{atm} + \phi_{noise}$ (1) where ϕ_{def} denotes the deformation phase of interest.

A. *Interferogram Formation*

An interferogram is generated by multiplying a master image with the complex conjugate of a slave image. This operation captures phase differences that represent path-length variations between two acquisitions. The wrapped phase is limited to the range ($-\pi$, $+\pi$), which introduces phase ambiguity [5].

$$I(x) = s_m(x) s_s^*(x) \quad (2)$$

$$\phi\_wrap(x) = arg(I(x)) \in (-\pi, \pi] \quad (3)$$

B. Flat-Earth Phase Removal

Due to the satellite's orbital geometry, a predictable flat earth phase component is introduced. This component must be removed before further processing to avoid masking subtle deformation signals [11].

$$\phi\_flat(x) = \frac{4\pi}{\lambda} \Delta R\_flat(x) \quad (4)$$

The unwrapped phase is converted to line-of-sight (LOS) displacement using the radar wavelength. For Sentinel-1 C band ($\lambda \approx 0.055$ m), one radian of phase corresponds to approximately 4.38 mm of LOS displacement [16].

$$d_{LOS}(x) = \phi_{uw}(x) \frac{\lambda}{4\pi} \quad (9)$$

I. Uncertainty Estimation

Every InSAR-derived displacement measurement carries inherent uncertainty due to atmospheric variability, orbital errors, and decorrelation. The phase standard deviation can be estimated as [1]

$$\sigma \approx \sqrt{\frac{1-(r)^2}{2(r)^2 L}} \quad (10)$$

I. RESULTS

The InSAR-derived displacement maps (Figs. 2, 3, 4, and 5) highlight distinct ground deformation patterns before and after the July 2025 Manali cloudburst. The results obtained from both ascending and descending Sentinel-1 datasets provide a comprehensive view of deformation characteristics along different line-of-sight (LOS) geometries

A. Pre-Event Deformation (May–June 2025)

The ascending track interferogram prior to the event(Fig.2) indicates relative stable terrain conditions, with only minor localized uplift zones (shown in blue) primarily concentrated along the valley slopes and ridge crests. These zones correspond to natural elastic adjustments and seasonal ground moisture variations. The average LOS displacement during this period remained within ±5 mm, suggesting limited deformation activity and high coherence (γ > 0.6) across most of the study area

G. Phase Unwrapping

Since radar phase repeats every 2π, the wrapped phase must be unwrapped to reconstruct the continuous deformation signal. Algorithms based on spatial continuity and coherence thresholds are applied to resolve phase ambiguities [13].

$$\phi_{uw}(x) = \phi_{wrap}(x) + 2\pi k(x), \quad k(x) \in Z \quad (8)$$

H. Phase to Displacement Conversion

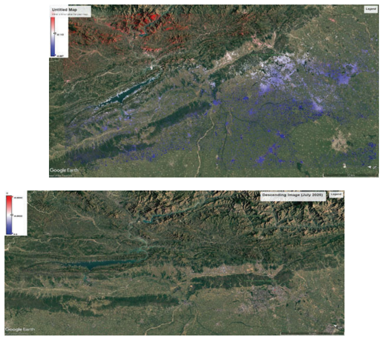

Fig. 2. Ascending track displacement map before the July 2025 Manali cloudburst (reference period: May–June 2025).

A. Post-Event Deformation (July–August 2025)

In contrast, the post-event displacement map (Fig. 3) reveals pronounced subsidence patterns (shown in red), particularly in the low-lying regions adjoining river channels, alluvial fans, and road cut slopes. Peak LOS subsidence reaches approximately 25–35 mm in some river-adjacent sectors. This deformation coincides spatially with areas of intense precipitation and observed slope failures, indicating that surface settlement was driven primarily by rapid soil saturation, slope collapse, and sediment compaction.

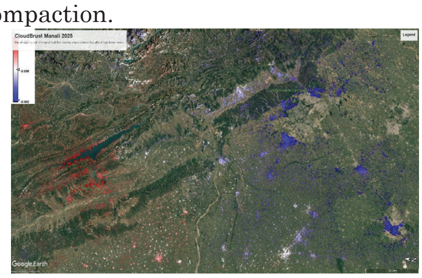

Fig. 3. Ascending track displacement map after the July 2025 Manali cloudburst (reference period: July–August 2025).

B. Descending Track Observations

The descending track interferograms provide complementary LOS perspectives. The June 2025 map (Fig. 4) supports the pre-event stability interpretation, showing minimal deformation with coherence values exceeding 0.7 in urban and rocky areas. After the event (Fig. 5), deformation patterns become more complex: pronounced subsidence (up to 30 mm) appears in valley bottoms, while minor uplift zones (upto +10 mm) emerge along ridge slopes, likely reflecting localized elastic rebound due to transient pore pressure changes.

Fig. 4. Descending track displacement map for June 2025 showing minimal pre-event deformation.

Fig. 5. Descending track displacement map for July 2025 highlighting deformation following the cloudburst.

C. *Interpretation of Deformation Patterns*

The spatial coincidence between deformation and geomorphic features reveals several insights:

- **Subsidence Zones:** These primarily align with steep, unconsolidated colluvial slopes and floodplains where saturation-induced compaction and shallow landsliding are prevalent. Settlements and roads along the Beas River valley fall within these critical deformation belts.
- **Uplift Zones:** Localized uplift patches, though limited in magnitude (<10 mm), likely result from short-term elastic recovery of slope materials or surface heave caused by differential water infiltration.
- **Deformation Complexity:** The contrast between ascending and descending LOS measurements suggests both vertical and horizontal motion components. This dual orbit approach enhances the interpretation of deformation geometry, a key advantage in mountainous environments.

D. *Overall Findings*

Comparative analysis of pre-post-event interferograms confirms a significant deformation anomaly induced by the July 2025 Manali cloudburst. While background seasonal motion remained modest (<5 mm), post-event displacement magnitudes exceeded 30 mm in affected zones. These f demonstrate a strong correlation between hydrological loading and surface response. The combination of high-resolution Sentinel-1 imagery and Differential InSAR processing thus proves effective for rapid assessment of rainfall-triggered ground instability in data-scarce Himalayan terrains.

This study highlights the operational potential of InSAR for near-real-time disaster monitoring. When integrated with rainfall intensity and hydrological data, such analyses can support early warning frameworks, infrastructure safety evaluations, and post-event hazard mapping in mountainous regions like Himachal Pradesh.

II. CONCLUSION

This study demonstrated the application of multi-temporal Sentinel-1 Interferometric Synthetic Aperture Radar (InSAR) for detecting and quantifying ground deformation associated with the July 2025 Manali cloudburst. Using a pairwise differential processing approach on ascending and descending track data, displacement maps were generated that revealed both localized subsidence and uplift across the Beas River valley. The results confirm that Sentinel-1 InSAR is a robust and efficient tool for capturing centimeter to millimeter-scale surface deformation in complex mountainous environments where ground surveys are often limited or unsafe.

Despite moderate coherence loss in snow-covered and vegetated areas, the analysis successfully delineated deformation hotspots near settlements, river terraces, and alluvial fans—zones that are highly sensitive to hydrological loading and slope instability. The maximum line-of-sight (LOS) displacement reached approximately 30–35 mm in subsiding regions, consistent with the spatial pattern of rainfall-induced slope failures observed after the event. These outcomes underscore the critical role of SAR-based techniques in improving disaster understanding and response in the

Himalayas.

The findings highlight the dual utility of InSAR: not only as a rapid post-disaster diagnostic tool but also as a potential near-real-time monitoring system for dynamic, hazard-prone regions. Future improvements can focus on integrating multiorbital observations to reconstruct three-dimensional displacement components, thereby improving the separation of vertical and horizontal motion. Additionally, coupling InSAR observations with hydrometeorological datasets and rainfall time series will provide deeper insights into the temporal evolution of deformation and its relation to extreme weather events.

Further refinement can be achieved by applying advanced time-series algorithms such as Persistent Scatterer InSAR (PSInSAR) and Small Baseline Subset (SBAS) methods to extend temporal coverage and reduce atmospheric noise. Integration with numerical slope stability and hydrological models could transform InSAR outputs into actionable risk assessments for infrastructure planning and early warning. Collectively, this research demonstrates the value of satellite-based geodetic monitoring for enhancing resilience in Himalayan environments facing accelerating climate-driven hazards.

ACKNOWLEDGMENT

The author expresses sincere gratitude to the Defence Institute of Advanced Technology (DIAT), Pune, for providing institutional support and funding through the internal research seed grant (Ref. DIAT/F/Adm/Project/OM/Corr/P-49). Appreciation is also extended to the Technology Innovation Hub on Autonomous Navigation (TiHAN), Indian Institute of Technology Hyderabad, for additional research assistance under project Ref. TiHAN-IITH/13/2023-24/399. The availability of Copernicus Sentinel-1 data from the European Space Agency (ESA) is gratefully acknowledged.

REFERENCES

[1] R. F. Hanssen, Radar Interferometry: Data Interpretation and Error Analysis. Dordrecht, The Netherlands: Springer, 2001.

[2] A. Ferretti, A. Fumagalli, F. Novali, C. Prati, F. Rocca, and A. Rucci, “A new algorithm for processing interferometric data-stacks: SqueeSAR,” IEEE Trans. Geosci. Remote Sens., vol. 49, no. 9, pp. 3460–3470, 2011.

[3] R. Bamler and P. Hartl, “Synthetic aperture radar interferometry,” Inverse Problems, vol. 14, no. 4, pp. R1–R54, 1998.

[4] F. Lattari, A. Rucci, and M. Matteucci, “A deep learning approach for change points detection in InSAR time series,” IEEE Trans. Geosci. Remote Sens., vol. 60, pp. 1–16, 2022.

[5] H. A. Zebker and R. M. Goldstein, “Topographic mapping from interferometric synthetic aperture radar observations,” J. Geophys. Res.: Solid Earth, vol. 91, no. B5, pp. 4993–4999, 1986.

[6] R. M. Goldstein and C. L. Werner, “Radar interferogram filtering for geophysical applications,” Geophys. Res. Lett., vol. 25, no. 21, pp. 4035–4038, 1998.

[7] R. Touzi, A. Lopes, J. Bruniquel, and P. W. Vachon, “Coherence estimation for SAR imagery,” IEEE Trans. Geosci. Remote Sens., vol. 37, no. 1, pp. 135–149, 1999.

[8] J. Cai, L. Zhang, J. Dong, J. Guo, Y. Wang, and M. Liao, “Automatic identification of active landslides over wide areas from time-series InSAR measurements using Faster R-CNN,” Int. J. Appl. Earth Observ. Geoinf., vol. 124, p. 103516, 2023.

[9] N. Anantrasirichai, J. Biggs, K. Kelevitz, Z. Sadeghi, T. Wright, J. Thompson, A. M. Achim, and D. Bull, “Detecting ground deformation in the built environment using sparse satellite InSAR data with a convolutional neural network,” IEEE Trans. Geosci. Remote Sens., vol. 59, no. 4, pp. 2940–2950, 2021.

[10] R. S. Kuzu, L. Bagaglini, Y. Wang, C. O. Dumitru, N. A. A. Braham, G. Pasquali, F. Santarelli, F. Trillo, S. Saha, and X. X. Zhu, “Automatic detection of building displacements through unsupervised learning from InSAR data,” IEEE J. Sel. Topics Appl. Earth Observ. Remote Sens., vol. 16, pp. 6931–6947, 2023.

[11] H. A. Zebker and J. Villasenor, “Decorrelation in interferometric radar echoes,” IEEE Trans. Geosci. Remote Sens., vol. 30, no. 5, pp. 950–959, 1992.

[12] A. Ferretti, C. Prati, and F. Rocca, “Nonlinear subsidence rate estimation using permanent scatterers in differential SAR interferometry,” IEEE Trans. Geosci. Remote Sens., vol. 38, no. 5, pp. 2202–2212, 2000.

[13] D. C. Ghiglia and M. D. Pritt, Two-Dimensional Phase Unwrapping: Theory, Algorithms, and Software. New York, NY, USA: Wiley, 1998.

[14] B. Rouet-Leduc, R. Jolivet, M. Dalaison, B. Riel, and M. Simons, “Autonomous extraction of millimeter-scale deformation in InSAR time series using deep learning,” Nature Commun., vol. 12, no. 1, pp. 6480, 2021.

[15] R. Burgmann, P. A. Rosen, and E. J. Fielding, “Synthetic aperture radar interferometry to measure Earth’s surface topography and its deformation,” Annu. Rev. Earth Planet. Sci., vol. 28, pp. 169.